Appl Biochem Biotechnol (2010) 162:2294–2312
DOI 10.1007/s12010-010-9003-3

Insights into pH-Induced Conformational Transition of β-Galactosidase from *Pisum sativum* Leading to its Multimerization

Alka Dwevedi · Vikash Kumar Dubey · Medicherla V. Jagannadham · Arvind M. Kayastha

Received: 5 March 2010 / Accepted: 25 May 2010 /
Published online: 13 June 2010

Abstract Although β-galactosidases are physiologically a very important enzyme and have may therapeutics applications, very little is known about the stability and the folding aspects of the enzyme. We have used β-galactosidase from *Pisum sativum* (*Ps*BGAL) as model system to investigate stability, folding, and function relationship of β-galactosidases. *Ps*BGAL is a vacuolar protein which has a tendency to multimerize at acidic pH with protein concentration ≥100 μg mL^{-1} and dissociates into its subunits above neutral pH. It exhibits maximum activity as well as stability under acidic conditions. Further, it has different conformational orientations and core secondary structures at different pH. Substantial predominance of β-content and interfacial interactions through Trp residues play crucial role in pH-dependent multimerization of enzyme. Equilibrium unfolding of *Ps*BGAL at acidic pH follows four-state model when monitored by changes in the secondary structure with two intermediates: one resembling to molten globule-like state while unfolding seen from activity and tertiary structure of *Ps*BGAL fits to two-state model. Unfolding of *Ps*BGAL at higher pH always follows two-state model. Furthermore, unfolding of *Ps*BGAL reveals that it has at least two domains: α/β barrel containing catalytic site and the other is rich in β-content responsible for enzyme multimerization.

Keywords *Ps*BGAL · Secondary structure · Intrinsic fluorescence · Hydrophobic domains

A. Dwevedi · A. M. Kayastha (✉)
School of Biotechnology, Faculty of Science, Banaras Hindu University, Varanasi 221005, India
e-mail: kayasthabhu@gmail.com

V. K. Dubey
Department of Biotechnology, Indian Institute of Technology Guwahati, Guwahati,
Assam 781039, India

M. V. Jagannadham
Molecular Biology Unit, Institute of Medical Sciences, Banaras Hindu University,
Varanasi 221005, India

Introduction

β-galactosidase catalyzes conversion of β-galactosides into monosaccharides. β-galactosidase is an essential enzyme in the human body. Deficiencies or impaired function of the enzyme results in lactose intolerance, galactosialidosis, Morquio B syndrome etc. Moreover, our group has reported purification, characterization, and immobilization of the enzyme from pea seeds [1, 2]. We have used β-galactosidase form *Pisum sativum* (*Ps*BGAL) as model system to understand folding of β-galactosidase in general and *Ps*BGAL in specific. The study may be useful in planning strategy against disease caused due to misfolding of human β-galactosidase and resulting loss of function. Moreover, it is also important to understand the factor responsible for oligomerization of proteins in functional native form and factors responsible for the regulation of association of subunits [3]. Among plant proteins, mainly proteases are extensively studied with respects to folding, and folding data on other plant proteins are limited [4].

BGAL present in eukaryotes (plants and animals) is a resident of acidic environment under *in vivo* conditions. It is present inside lysosomes (in animals, pH ~5.0) and vacuoles (in plants, pH ~5.0). It was suggested that the multimerization might be a crucial factor in its stabilization under *in vivo* conditions [5–8]. Further studies on enzymes residing in acidic environment under *in vivo* conditions like α-galactosidases, β-D-glucosidases, β-*N*-acetylhexosaminidases, and α-glucosidases isolated from plant vacuoles were also found to undergo multimerization [9–12]. It was found in case of plant α-galactosidases that the enzyme (glycoprotein) contains two sites: *hydrolase* and *lectin*. Site containing lectin binds to the adjacent glycan moiety present in the enzyme leading to its multimerization [9, 13–15]. It was elucidated that similar mechanism might have existed in case of BGAL too due to the presence of lectin-like domain in the enzyme [16]. Later, it was found that there are two broad classes of BGAL based on primary sequence analysis: presence and absence of lectin domain at C-terminus of the enzyme. *Ps*BGAL isolated from seeds of *P. sativum* was found to be devoid of lectin [1]. The present work is based on probing the presence of pH-dependent multimerization and further elucidating its mechanism and significance. The similar approach is used for elucidating folding mechanism of proteases [17].

A number of studies have examined the attributes of protein binding sites present in protein–protein complex. Binding site interfaces are highly hydrophobic, and the majority of backbone hydrogen bonds are completely wrapped intramolecularly by non-polar groups except for a few likely to be around the binding site [18]. The insufficiently dehydrated hydrogen bonds may be dramatically stabilized on binding. Alanine scanning of protein–protein interfaces has shown that the binding free energy is not equally distributed at the binding interface. Rather, there are hot spots of binding energy consisting of a subset of residues at the interface [19]. Systematic analysis has found the hot spots to be particularly enriched in Trp, Tyr, and Arg. These were largely surrounded by hydrophobic rings, probably to occlude bulk solvent [20]. These hot spots are likely to be conserved, and these structurally conserved residues differentiate between binding sites and the remainder of the molecular surface [21]. Moreover, binding mechanism of protein–protein interaction is robust and is governed by protein topology [22]. A deep insight into the mechanism of protein–protein interaction would help to understand various biological processes (like virus assembly, importantly in life cycle of lentivirus, adenovirus, cytomegalovirus, herpes simplex virus, etc.) that require protein multimerization. A US Patent 6653443 has been developed which is based on effectively blocking multimerization of HIV-1 viral protein Vif, thus preventing completion of virus life cycle.

The present work reports the folding studies of β-galactosidase isolated from pea seeds (*Ps*BGAL), thus helpful in understanding various diseases caused due to enzyme deficiency and malfunctioning. Further, helpful in successful commercial implementation of *Ps*BGAL in production of lactose hydrolyzed milk and milk derived products.

Materials and Methods

Chemicals

All the chemicals for buffers and other reagents were of analytical grade or electrophoresis grade. Unless stated, all the chemicals were purchased from Sigma (St. Louis, MO, USA). Milli-Q quality water with resistance of higher than 18 MΩ cm^{-1}(at 25 °C) was used throughout the experiments.

Buffers, Denaturants, and Solutions

The buffers used in the study were 10 mM glycine-HCl (pH 2.0–4.5), sodium acetate-acetic acid (pH 5.0–6.0), sodium phosphate monobasic-sodium phosphate dibasic (pH 6.5–7.5), and Tris–HCl (pH 8.0–9.0). All the buffers contained 0.02 mM EDTA and 1 mM DTT. DTT was used to avoid any complication due to interaction of thiol groups in the protein. Stock solution of GdnHCl was freshly prepared, and the molarity of the solution was determined by density measurements [23]. All solutions in fluorescence and CD studies were filtered through 0.45 μm filter prior to use.

Enzyme Preparation

*Ps*BGAL was isolated and purified from seeds of *P. sativum* to homogeneity using four steps (acid precipitation, ammonium sulfate fractionation, hydrophobic interaction chromatography, and ion exchange chromatography). Final preparation was 910-folds purified with a specific activity of 77.33 μmoL min^{-1} mg^{-1} and was found to be homogeneous on sodium dodecyl sulfate-polyacrylamide gel electrophoresis [17].

Enzyme Assay

The activity against *o*-nitrophenyl-β-D-galactopyranoside (ONPG) was assayed by incubating 450 μL of ONPG solution (22.22 mM) prepared in 50 mM glycine-HCl buffer (pH 3.2) with 50 μL of suitably diluted enzyme for 5 min at 37 °C. Reaction was terminated by adding 1.5 mL of sodium tetraborate solution (20 mM), and the absorbance was recorded at 405 nm. One unit of BGAL activity was defined as the amount of enzyme required for releasing 1 μmoL of *o*-nitrophenol produced min^{-1} mL^{-1} at 37 °C. Extinction coefficient of *o*-nitrophenol used during calculation was 4.05×10^3 M^{-1} cm^{-1}.

Protein Assay

Protein was estimated as described by Bradford [24] with the Bradford reagent, calibrated with crystalline bovine serum albumin.

Size Exclusion Chromatography (SEC)

Size exclusion chromatography (SEC) was carried out using Superdex S-200 HR 10/30 column on an automated AKTA fast protein liquid chromatography (Amersham Biosciences, Inc., Piscataway, NJ, USA). Column was calibrated with markers of molecular mass 440, 206, 66, and 43 kD (Amersham Biosciences) before use. Column was equilibrated at pH 7.0 using sodium phosphate buffer (50 mM) containing 0.1 M NaCl with each marker having protein concentration of 1 mg mL^{-1}. A standard plot of log molecular mass versus elution volume was generated to extrapolate the molecular mass of protein sample to be determined. For broader peak, center of the peak was taken. pH-induced changes in *Ps*BGAL were studied by equilibrating the column and dialyzing the enzyme overnight at the respective pH.

Spectroscopic Measurements

Spectropolarimetric measurements were done on a JASCO J 500A spectropolarimeter equipped with a constant temperature cell holder. The instrument was calibrated using ammonium (+)-10-camphorsulfonate. Temperature of the cell holder was set at 25 °C using Julabo F 25 water bath. Spectra in the near-UV region (between 320 and 260 nm) or in the far-UV region (260–200 nm) were collected using a 10- or 1-mm path length cell, respectively, with a scan speed of 5 nm min^{-1}. Five consecutive scans were taken for each sample, the reference spectra of the respective media subtracted and the data averaged to reduce noise. The protein was equilibrated in buffers of pH 5.0 and 8.0 as well as in the indicated amounts of GdnHCl. After subtracting appropriate blanks, mean residue ellipticities were calculated, using the formula:

$$[\theta] = \theta_{\text{obs}} \times \text{MRW}/10cl, \tag{1}$$

where θ_{obs} is the observed ellipticity in degrees, MRW is the mean residue weight, c is the concentration of protein (g cm^{-3}), and l is the path length in centimeters [25]. A mean residue molecular weight 110 was used. All far-UV measurements were done with sensitivity 0.5 m^{o} cm^{-1}.

Fluorescence measurements were carried out on a Perkin-Elmer LS-50B spectrofluorimeter equipped with a constant temperature (25 °C) cell holder. Tryptophan was selectively excited at 292 nm, and the emission was recorded from 300 to 400 nm with 5-nm slit width for both excitation and emission. All measurements were corrected for background signal. The average emission wavelength was calculated for each fluorescence emission scan using Eq. 2:

$$\langle\lambda\rangle = \sum_{i=1}^{N} (I_i\lambda_i) / \sum_{i=1}^{N} (I_i), \tag{2}$$

where $<\lambda>$ is the average emission wavelength, and I_i is the fluorescence emission at wavelength λ_i.

ANS Binding Assay

Exposure of hydrophobic surfaces in the enzyme was measured by its ability to bind to the fluorescent dye ANS [26]. A stock solution of ANS was prepared in methanol, and the dye

concentration was determined using an extinction coefficient of ε=5,000 M^{-1} cm^{-1} at 350 nm [27]. ANS binding saturation to *Ps*BGAL (200 μg mL^{-1}) was determined by plotting ANS fluorescence intensity at 475 nm versus varying concentration of ANS (0 to 50 μM). Fluorescence of ANS was excited at 380 nm, and emission spectra were recorded between 400 and 600 nm with 5-nm slit width for both excitation and emission. Using the equation:

$$y = \frac{y_{\max}[\mathrm{ANS}]}{k_d + [\mathrm{ANS}]} \tag{3}$$

k_d (binding constant) was determined, which was found to be 28 μM (data not shown). All experiments based on ANS binding studies were performed by incubating protein with 1 mM ANS for more than 30 min at room temperature in the dark.

Denaturant-Induced Equilibrium Studies

Unfolding of *Ps*BGAL was studied using denaturant GdnHCl at pH 5.0 and 8.0. Mixture of protein samples (*Ps*BGAL) and GdnHCl were prepared to finally achieve constant protein concentration (200 μg mL^{-1}), while concentrations of denaturant were varied from 0 to 6 M. Final concentration of the protein and denaturant in each sample were determined by Bradford method and refractive index measurements, respectively. Denaturant containing protein samples were incubated at pH 5.0 and 8.0 for 2 h at 25 °C to attain equilibrium. Protein samples were thoroughly mixed, centrifuged, and filtered before doing unfolding experiments. Unfolding of samples was analyzed using far-UV CD spectral studies in the wavelength range 200–260 nm for secondary structural changes, intrinsic Trp emission fluorescence measured by excitation of sample at 292 nm for local or tertiary change and changes in enzyme activity for tertiary as well changes around active site of enzyme.

Unfolding Data Analyses

Using data obtained from equilibrium studies, determination of fraction unfolded, equilibrium constant, and free energy can be calculated. The mathematic models were adopted and modified according to previous report [28]. The apparent unfolded state at a given GdnHCl concentration, F[GdnHCl] is given by following equations:

$$F[\mathrm{GdnHCl}] = \sum_{i=1}^{N} X_i F_i \tag{4}$$

$$F_i = F_0 + S_i[\mathrm{GdnHCl}] \tag{5}$$

where X_i is the mole fraction, and F_i is the spectral parameter of state i. The X_i values are calculated for different models (far-UV CD, Trp fluorescence and enzyme activity using ONPG as substrate). In case of far-UV CD, changes taking place in MRW ellipticities were monitored at 222 nm, as CD spectroscopy is most sensitive to changes taking place in α-helix [23]. Percentage of α-helical content was found using SOMCD available at http://somcd.geneura.org. Intrinsic Trp fluorescence intensity changes during unfolding were monitored at 355 nm. F_0 is the parameter of i-state in the absence of denaturant, i.e., native protein, and slope S_i is dependence of F_i on denaturant concentration.

The changes taking place in free energy with unfolding is given as described with assumption of linear dependence of ΔG_i^0 on the concentration of GdnHCl.

$$\Delta G_i = \Delta G_i^0 - m_i[\text{GdnHCl}] = -RT \ln K_i \tag{6}$$

where ΔG_i is the free energy change for unfolding, and ΔG_i^0 is the free energy change in the absence of denaturant. K_i is the equilibrium constant, and m_i reflects the sensitivity of the transition to denaturant concentration. We have referred value of ΔG_i in the presence of denaturant and ΔG_i^0 in the absence of denaturant at 298 K. R is a gas constant whose value was taken as 1.99 cal moL^{-1} K^{-1} during various calculations. It is worth mentioning that control experiments demonstrated reversibility of oligomer dissociation and unfolding.

Four-State Model

In this model, the protein is assumed to be either in the native monomeric state (N) or in the unfolded monomeric state (U), and I_1 and I_2 are two unfolding intermediates. Four-state equilibrium model is represented as follows:

$$N \overset{K_1}{\leftrightarrow} I_1 \overset{K_2}{\leftrightarrow} I_2 \overset{K_3}{\leftrightarrow} U \tag{7}$$

K_1, K_2, and K_3 are the equilibrium constants for the three steps, respectively. The equations describing the thermodynamics of this model are as follows:

$$K_1 = [I_1]/[N];\ K_2 = [I_2]/[I_1];\ K_3 = [U]/[I_2] \tag{8}$$

$$Q = 1 + K_1 + K_1K_2 \tag{9}$$

$$X_\text{N} = 1/Q;\ X_1 = K_1/Q;\ X_2 = K_1 \cdot K_2/Q;\ X_\text{U} = K_1 \cdot K_2 \cdot K_3/Q \tag{10}$$

$$\begin{aligned}\Delta G_1 = \Delta G_1^0 - m_1 D = -RT \ln K_1;\ \Delta G_2 = \Delta G_2^0 - m_2 D = -RT \ln K_2;\ \Delta G_3 \\ = \Delta G_3^0 - m_3 D = -RT \ln K_3\end{aligned} \tag{11}$$

where Q is the partition function, and X_N, X_1, X_2, and X_U are mole fractions of the proteins in the native, intermediates, and unfolded state, respectively. ΔG_1, ΔG_2, and ΔG_3 are standard free energy changes for the unfolding transition in the presence of denaturant (D), while ΔG_1^0, ΔG_2^0, and ΔG_3^0 are standard free energy changes for the unfolding transition in the absence of denaturant (D), respectively. m_1, m_2, and m_3 are the denaturant susceptibility parameters that describe the dependence of standard energy on denaturant concentration.

Thus, in this case, Eq. 3 can be written as

$$F(D) = X_\text{N}F_\text{N} + X_1F_1 + X_2F_2 + X_\text{U}F_\text{U} \tag{12}$$

where F_N and F_U are parameters of N and U states, respectively, and F_1 and F_2 are parameters for intermediate states. A non-linear least-squares fitting program using Origin 7.0 (Microcal Software Inc.) will yield the free energy differences between the native form

and the intermediate, ΔG_1^0; between subsequent intermediates, ΔG_2^0; and between intermediate and unfolded states, ΔG_3^0 as well as m_1, m_2, and m_3. Therefore, the entire denaturation curve can be represented in terms of two variables $F(D)$ and $[D]$ as follows (Eq. 13):

$$F(D)=\frac{F_N+F_1\exp-\left(\Delta G_1^0-m_1D\right)+F_2\exp-\left[\Delta G_1^0+\Delta G_2^0-(m_1+m_2)D\right]+F_U\exp-\left[\Delta G_1^0+\Delta G_2^0+\Delta G_3^0-(m_1+m_2+m_3)D\right]}{1+\exp-\left(\Delta G_1^0-m_1D\right)+\exp-\left[\Delta G_1^0+\Delta G_2^0-(m_1+m_2)D\right]+\exp-\left[\Delta G_1^0+\Delta G_2^0+\Delta G_3^0-(m_1+m_2+m_3)D\right]} \tag{13}$$

Two-State Model

In this model, the protein is assumed to be either in the native monomeric state (N) or in an unfolded monomeric state (U), and K_{eq} is the equilibrium constant for the transition. It is represented by

$$N \underset{}{\overset{Keq}{\rightleftarrows}} U \tag{14}$$

Similarly, the following equations are derived as above:

$$K_{eq} = [U]/[N] \tag{15}$$

$$Q = 1 + K_{eq} \tag{16}$$

$$X_N = 1/Q,\ X_U = K_{eq}/Q \tag{17}$$

$$\Delta G = \Delta G^0 - mD = -RT \ln K_{eq} \tag{18}$$

Thus, Eq. 3 becomes as follows in this case:

$$F(D) = X_N F_N + X_U F_U \tag{19}$$

where F_N and F_U are native and unfolded states, respectively. A non-linear least-squares fitting program using Origin 7.0 (Microcal Software Inc.) will yield the free energy difference in the absence of denaturant ΔG^0 and "m." Substituting all parameters including free energy, equilibrium constant in Eq. 19, the entire denaturation curve can be represented as

$$F(D) = \frac{F_N + F_U \exp -(\Delta G^0 - mD)}{1 + \exp -(\Delta G^0 - mD)} \tag{20}$$

Control experiments on the enzyme demonstrated reversibility of oligomer dissociation and unfolding.

Results and Discussion

pH-Induced Multimerization

*Ps*BGAL was most stable and contains maximum activity (μmoL min^{-1} mg^{-1}) at protein concentrations ranging from 100 to 1,000 μg mL^{-1} at acidic pH (Fig. 1a). Stability of *Ps*BGAL (at acidic pH, particularly vacuolar pH) reduces drastically when protein concentration was <100 μg mL^{-1} [17]. *Ps*BGAL (200 μg mL^{-1}) exists at different state of multimers at different pH: pH 5.0, tetramer (228.3 kD); pH 6.0, trimer (173.6 kD) and dimer (112.1 kD); pH 7.0, dimer (110.2 kD); and at pH 8.0 and 9.0, monomer (57 kD), as observed using SEC (Fig. 1b). The SEC profiles show symmetrical but broad peaks, indicating minor oligomeric heterogeneity. State of *Ps*BGAL multimerization at pH 5.0 (vacuolar pH) was dependent on protein concentrations: 80 μg mL^{-1} (<100 μg mL^{-1}), monomer (57.2 kD); 100–300 μg mL^{-1}, tetramer (228.3 kD); 400 μg mL^{-1}, enzyme came into void volume. Studies at alkaline pH (pH 8.0) showed no change in SEC protein profiles at different protein concentrations (data not shown). We have carried out our further studies at pH 5.0 and pH 8.0 to study about the phenomenon of pH-induced multimerization.

Secondary Structure Analysis

The alterations in secondary structure of *Ps*BGAL at pH 5.0 and pH 8.0 were analyzed by using far-UV CD spectra. There was negligible qualitative change in the CD spectra at protein concentrations ranging from 100 to 300 μg mL^{-1} at pH 5.0 and 8.0, respectively (data not shown). Noise to signal ratio was much intense in case of *Ps*BGAL with a protein concentration >300 μg mL^{-1} at pH 5.0, due to which spectra could not be recorded beyond 215 nm. Figure 2, showed far-UV CD spectra of *Ps*BGAL (protein concentration, 100 μg mL^{-1}) at pH 5.0 and 8.0, respectively. According to CD spectra at pH 5.0, two prominent negative peaks at 211 and 223 nm were observed with minimum at 223 nm. At pH 8.0, two negative prominent peaks are at 206 and 219 nm with minimum at 206 nm. Presence of two negative unequal peaks obtained from far-UV CD spectra at 208 and 222 nm corresponds to presence of both α and β structures in the protein. Minimum observed at 222 nm corresponds to α/β barrels, while minimum at 208 nm corresponds to existence of $\alpha+\beta$ structures in the protein [29]. It can be concluded from present far-UV CD spectra that *Ps*BGAL has α/β and $\alpha+\beta$ structures at pH 5.0 and 8.0, respectively, with deviation of ~2 nm (standard error, ≤1%) corresponding to experimental variability during measurements at the respective wavelength. The total estimation of percentage of α-helix, percentage of β-strand, and percentage of random coils present in *Ps*BGAL at pH 5.0 and 8.0 were calculated using SOMCD available at http://somcd.geneura.org based on Kohonen's self-organizing maps (SOM). Table 1 shows the percentage of secondary structures present in *Ps*BGAL at two respective pH. There was an appearance of β-sheet and decrease in α-helical content by ~15%, while no change was observed in turns and random coils as the pH was increased from 5.0 to 8.0. It can be concluded that increase in β-content at pH 5.0 is one of the crucial factor involved in self-aggregation of *Ps*BGAL.

Fig. 1 **a** Effect of pH on *Ps*BGAL at different protein concentrations. *Marked circular region* showed maximum depression with respect to other places, representing the region corresponding to maximum stability of *Ps*BGAL. **b** Gel permeation of *Ps*BGAL at different pH. Of protein at different pH (pH 5.0 to 9.0), 200 μg mL^{-1} were loaded onto the column pre-equilibrated at respective pH ▶

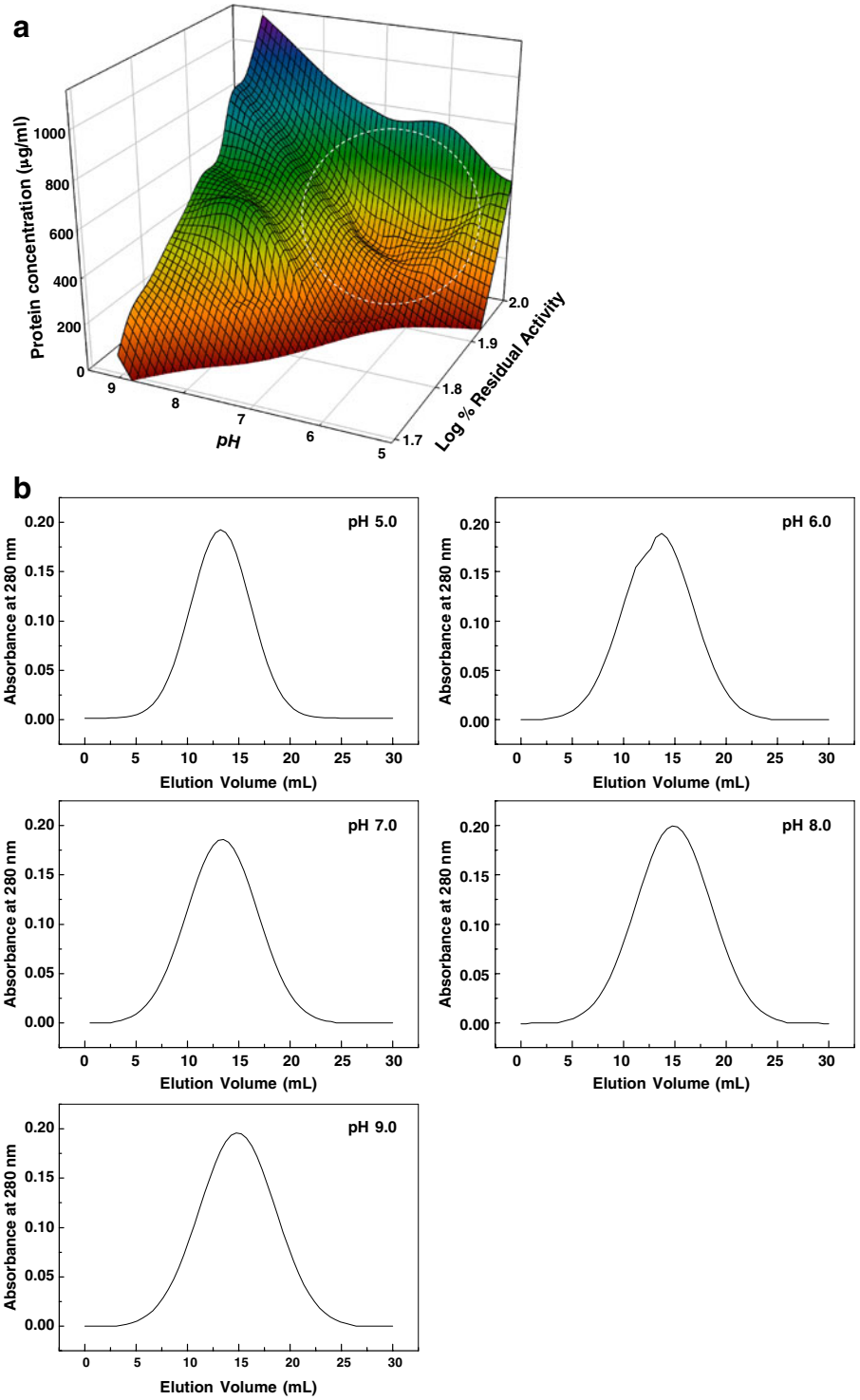
a
Protein concentration (µg/ml)
1000
800
600
400
200
0
9
8
7
6
5
pH
1.7
1.8
1.9
2.0
Log % Residual Activity
b
pH 5.0
pH 6.0
pH 7.0
pH 8.0
pH 9.0
Absorbance at 280 nm
0.20
0.15
0.10
0.05
0.00
0
5
10
15
20
25
30
Elution Volume (mL)

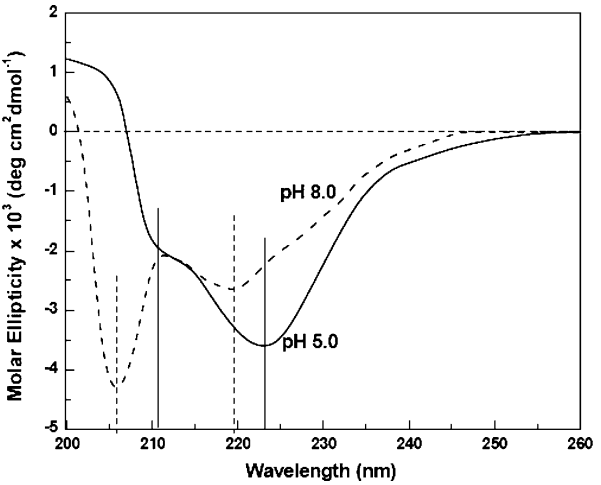

Fig. 2 Secondary structure of *Ps*BGAL as a function of pH. Far-UV CD spectra of *Ps*BGAL (obtained by dialyzing against the respective pH for 24 h at 4 °C) at pH 5.0 and 8.0 with a protein concentration of 100 μg mL^{-1}

Changes in percentage of secondary structures with pH have also been reported by various researchers. It was reported that Annexin VI (Anx VI) has 80±22% α-helical content at pH 7.4 [30]. As the pH was lowered to 3.0, it resulted in the decrease of α-helical and the appearance of new β-structures (23±2%) and also an increase in the number of β-turn segments within the Anx VI molecule, as compared with pH 7.4. pH-Induced changes in secondary structures were possibly a mechanism used to neutralize charge that renders the surface of protein more hydrophobic. This leads to movement of domains to form new β-sheet structures, due to which, protein–protein interactions were favored. In case of G protein, as the pH was lowered from 7.6 to 5.6, there was approximately 56% loss in α-helical content [31]. Similarly, pulmonary surfactant protein A and scrapie prion protein undergo progressive decrease in α-helical content and increase in β-sheet upon acidification [32, 33]. Alkaline pH has led to conformational change from β-sheet→α-helix transition. They have suitably reasoned that changes in secondary structures at varying pH were due to changes in ionization of –R groups of amino acids depending on their respective pI. Like in aqueous buffer, Ala peptide (AA9) shows maximum helical content at neutral pH, and the helicity decreases at both basic and acidic pH, which is the result of protonation of the side chains of glutamic residues at acidic pH and deprotonation of the side chains of lysine residues at basic pH [34]. Therefore, it can be concluded that multimerization of *Ps*BGAL present at pH 5.0 might be due to increased β-content leading to self-induced aggregation at the respective pH.

Changes in Intrinsic Fluorescence

Residues like Trp, Tyr, and Phe are important in intrinsic fluorescence of a protein. These residues are surrounded by non-polar environment. Trp is the most sensitive residue to its

Table 1 Percent of secondary structures present in *Ps*BGAL at different pH.

Percent secondary structures	H 5.0	pH 8.0
α-Helix	33.6±2.8	48.4±3.1
β-Sheet	26.6±1.0	11.1±1.1
Turns	11.0±1.3	11.4±1.3
Random coil	28.8±2.1	29.1±2.4

The content of secondary structures was calculated from CD data by SOMCD program.

local environment with respect to other two residues. Changes in emission spectra of tryptophan are observed in response to protein conformational transitions, subunit association, substrate binding, or denaturation affecting the local environment surrounding the indole ring. Various reports have revealed that Trp is one of the conserved residues of hydrophobic interfaces present at the binding sites and is important in protein–protein associations [19, 20, 35].

Conformational change undergone by *Ps*BGAL was studied at pH 5.0 and 8.0 as a function of protein concentrations in the range 20 to 100 μg mL^{-1} (Fig. 3a). *Ps*BGAL showed significant change at pH 5.0 with increase in fluorescence intensity by 32.2% as the protein concentration was increased from 20 to 100 μg mL^{-1}. There was negligible increment of fluorescence intensity by 0.33% which was observed at pH 8.0 with increasing protein concentrations. *Ps*BGAL was monomeric when the protein concentration was <100 μg mL^{-1}, and multimerization occurred as the protein concentration was ≥100 μg mL^{-1} at pH 5.0 (gel permeation studies, "pH-Induced Multimerization" section). Thus, it can be concluded that conformational change undergone by the enzyme was accompanied with the burial of its Trp containing moiety under acidic conditions with increasing protein concentrations. Therefore,

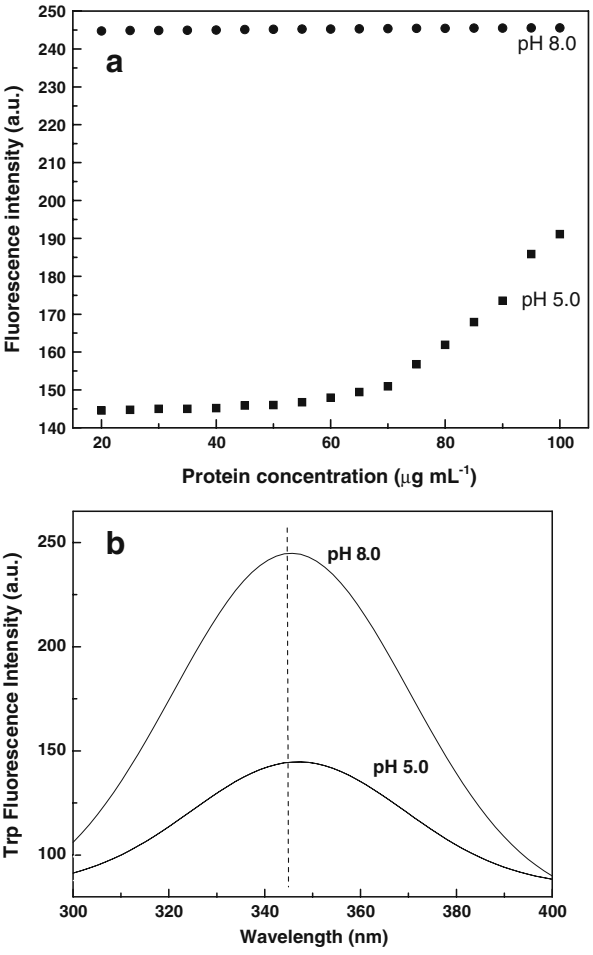

Fig. 3 Intrinsic Trp fluorescence of *Ps*BGAL (excitation at 292 nm) as a function of protein concentration. **a** Effect of protein (*Ps*BGAL) concentration on fluorescence intensity at pH 5.0 and 8.0. **b** Fluorescence spectra of *Ps*BGAL (20 μg mL^{-1}) at pH 5.0 and 8.0

this might be the preparative step for enzyme multimerization at higher protein concentrations under acidic conditions.

Comparative studies were carried at pH 5.0 and 8.0 using protein concentration of 20 μg mL^{-1} by intrinsic fluorescence studies. A negligible blue shift of 1.7 nm with drastic increase in fluorescence intensity by ~69% was observed at pH 8.0 with respect to pH 5.0 (Fig. 3b). The presence of various quenchers around Trp residues might be responsible for lowering the fluorescence intensity at pH 5.0. Most probably, imidazole ring of histidine residue (pK_a, 6.0), which is the strongest quencher in its cationic form [36], is responsible for considerable lowering of fluorescence intensity at pH 5.0 than at pH 8.0. It also supports that conformational change is undergone by *Ps*BGAL on acidification due to loss of α-helical structure leading to exposure of Trp residues to polar environment [37].

Exposure of Hydrophobic Clusters and Patches

Exposure of hydrophobic segments of *Ps*BGAL at pH 5.0 and pH 8.0 was probed by measuring ANS binding. This fluorescent compound binds strongly to cationic groups of proteins and polyamino acids through ion pair formation. It is a much utilized fluorescent "hydrophobic probe" for examining the non-polar character of proteins and membranes. ANS binding is accompanied by a large increase in its fluorescence quantum yield and relative blue shift in emission spectra [38].

*Ps*BGAL multimerizes as the protein concentration was ≥100 μg mL^{-1} under acidic conditions ("pH-Induced Multimerization" section). Thus, role of hydrophobic clusters present in the enzyme multimerization can be studied using ANS binding based on their exposure on subsequent monomerization. *Ps*BGAL with protein concentrations in the range 20 to 100 μg mL^{-1} at pH 5.0 and 8.0 was taken for the present study. There was insignificant change in ANS fluorescence intensity and wavelength maximum at pH 5.0 and 8.0 with increasing protein concentrations at the respective pH (data not shown). It can be concluded that hydrophobic clusters present in the enzyme do not contribute to multimerization as a function of protein concentrations.

Comparative analyses of *Ps*BGAL at pH 5.0 and 8.0 were done using ANS binding studies at protein concentration of 20 μg mL^{-1}, which correspond to maximum ANS fluorescence intensity. It was observed that there was an increase in ANS binding as the *Ps*BGAL was acidified from pH 8.0 to pH 5.0. A blue shift in λ_{max} of ~20 nm with an increase in fluorescence intensity by ~20% was observed on *Ps*BGAL acidification (Fig. 4). Thus, the enzyme has higher surface hydrophobicity at acidic pH than at higher pH. It concludes with support of secondary structure analysis ("Secondary Structure Analysis" section) and intrinsic fluorescence studies ("Changes in Intrinsic Fluorescence" section) that *Ps*BGAL has entirely different conformational orientation at different pH.

Unfolding Studies at Acidic pH

These studies would reveal the mechanism of *Ps*BGAL multimerization at pH 5.0. Unfolding studies of *Ps*BGAL (using GdnHCl) were monitored by conformational changes using intrinsic Trp fluorescence, secondary structural studies using far-UV CD (200–260 nm), and enzyme activity studies. Fraction unfolded (f_u) were determined by decrease in intrinsic Trp fluorescence intensity at 355 nm, loss in α-helical content corresponding to θ_{222} of far-UV CD spectra, and loss in enzyme activity. A plot of fraction unfolded (f_u) versus varying concentration of GdnHCl was generated (Fig. 5a) based on studies of intrinsic Trp fluorescence, far-UV CD, and enzyme activity. Unfolding of *Ps*BGAL was

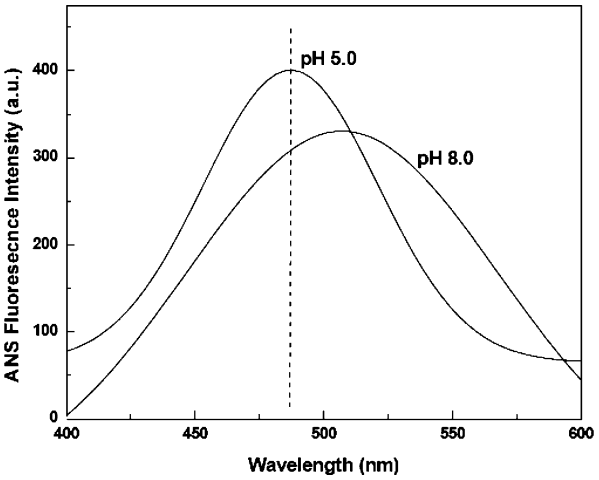

Fig. 4 ANS binding of *Ps*BGAL (excitation at 380 nm) as a function of protein concentration. ANS binding of *Ps*BGAL (20 μg mL^{-1}) at pH 5.0 and 8.0

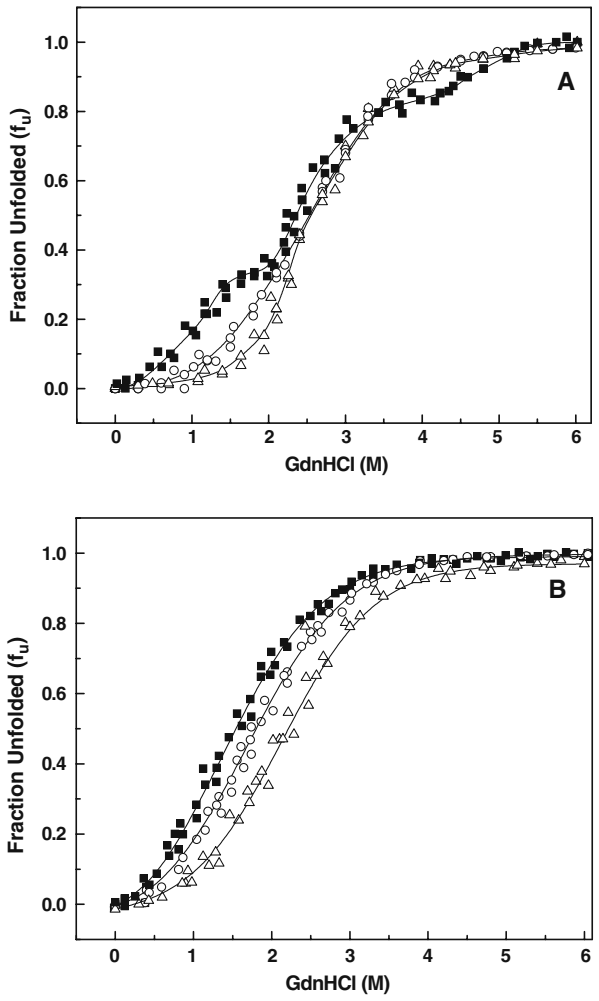

Fig. 5 Unfolding of *Ps*BGAL (200 μg mL^{-1}) by GdnHCl at different pH. Changes in the conformations are monitored by θ_{222} (*squares*), intrinsic Trp fluorescence intensity corresponding to emission at 355 nm (*circles*), and enzymatic activity (*triangles*) at pH 5.0 (**a**) and 8.0 (**b**). Data corresponding to circular dichroism, fluorescence, and enzyme activity were obtained from three independent experiments and fitted using Eqs. 13 and 20 as described in "Materials and Methods" section

found to be a cooperative process, and data obtained by three studies were non-coincidental. Data obtained by three studies were fitted using non-linear fit program of Origin 7.0 software based on Eqs. 13 (four-state model) and 20 (two-state model), respectively.

Four states were obtained on unfolding of *Ps*BGAL corresponding to secondary structural studies based on loss in α-helical content: N (native protein), I_1 (first intermediate), I_2 (second intermediate), and U (completely unfolded). Transition mid-points, $N \leftrightarrow I_1$, $I_1 \leftrightarrow I_2$, and $I_2 \leftrightarrow U$, were 1.07, 2.68, and 4.93 M, respectively. Thermodynamic parameters including conformational free energy and cooperativity index were obtained using linear extrapolation model based on Eqs. 7–10 and are given in Table 2. Conformational free energy change from state $N \leftrightarrow I_1$ was 2.57 kcal moL^{-1} M^{-1} (Table 2), much lesser than the other naturally occurring proteins. In contrast to states $I_1 \leftrightarrow I_2$ and $I_2 \leftrightarrow U$, conformational free energy corresponds to 11.03 and 13.95 kcal moL^{-1} M^{-1} (Table 2), respectively (lying in the range as reported earlier in case of other globular proteins [39]). Total conformational free energy $\left(\Delta G_1^0 + \Delta G_2^0 + \Delta G_3^0\right)$ of native *Ps*BGAL at pH 5.0 was found to be 27.55±0.97 kcal moL^{-1} M^{-1}.

According to intrinsic Trp fluorescence and enzyme activity studies, two forms, N (native protein) and U (completely unfolded), were dominated. Transition mid-point $N \leftrightarrow U$, obtained from two studies, was found to be similar with value corresponding to 2.54 M. Thermodynamical parameters obtained from linear extrapolation models described in "Materials and Methods" section (Eqs. 14–17) are given in Table 2. Total conformational free energy of native *Ps*BGAL was found to be 5.26±0.94 kcal moL^{-1} M^{-1} from enzyme activity studies, whereas it was 4.88±0.25 kcal moL^{-1} M^{-1} as found from intrinsic Trp fluorescence studies. Conformational energy obtained from far-UV CD, intrinsic Trp fluorescence, as well as enzyme activity studies suggests that secondary structures were much more conserved and resistant to denaturation by GdnHCl.

Characterization of Four States (N, I_1, I_2, and U) Obtained from Secondary Structural Studies on Unfolding of PsBGAL (200 μg mL^{-1})

*Native state (N) Ps*BGAL in the N state completely retained its tertiary structure, corresponding to a positive peak centered at 278 nm and a negative peak between 298 and 300 nm of near-UV CD spectra (Fig. 6b). N state of *Ps*BGAL corresponding to protein concentration of 200 μg mL^{-1} was tetrameric ("pH-Induced Multimerization" section).

Table 2 Thermodynamic parameters of *Ps*BGAL at different pH.

Parameters		Free energy (kcal moL^{-1} M^{-1})			Cooperativity index (kcal moL^{-1} M^{-1})		
		ΔG_1^0	ΔG_2^0	ΔG_3^0	m_1	m_2	m_3
Far-UV CD	pH 5.0	2.57±0.00	11.03±0.05	13.95±0.92	2.50±0.00	4.12±0.31	2.83±0.96
	pH 8.0		4.14±0.61			1.84±0.27	
Trp fluorescence	pH 5.0		4.88±0.25			1.92±0.10	
	pH 8.0		2.07±0.30			1.16±0.17	
Enzymatic activity	pH 5.0		5.26±0.94			2.07±0.37	
	pH 8.0		1.89±0.18			1.26±0.12	

Obtained using linear extrapolation plots based on Eqs. (7–11) and (14–19) as given in "Materials and Methods" section.

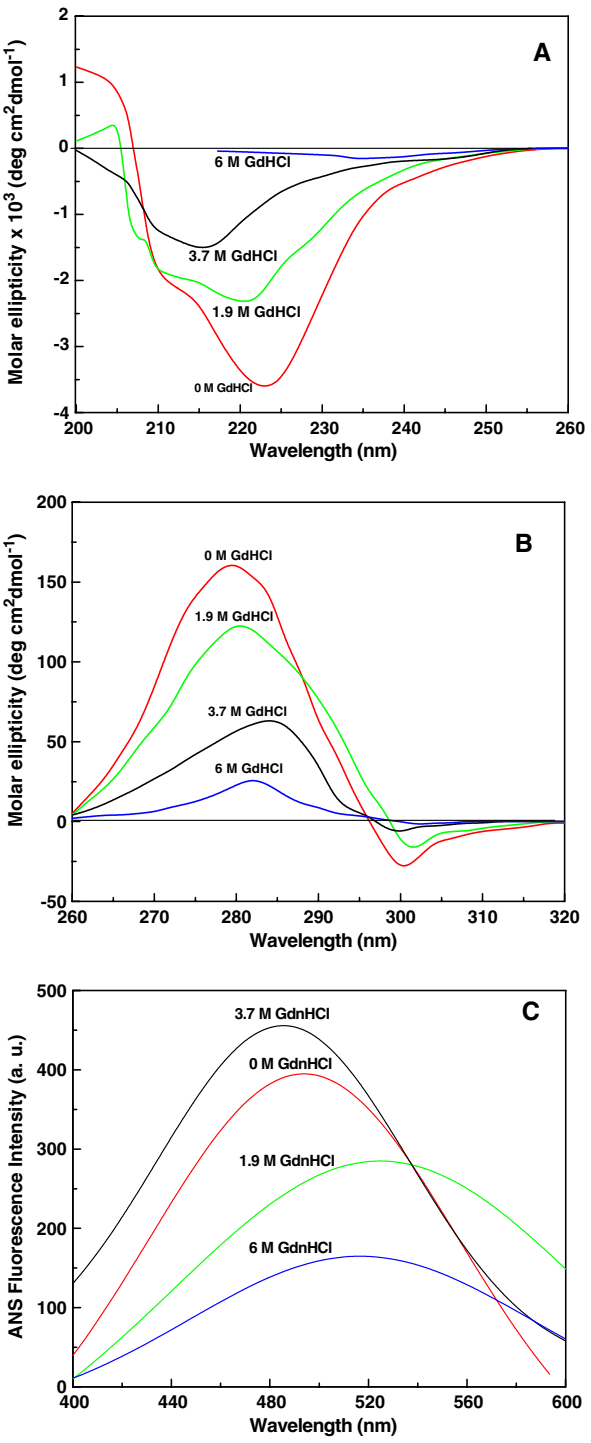

Fig. 6 Secondary and tertiary studies of *Ps*BGAL at varied concentration of GdnHCl. Far-UV CD spectra (**a**) and near-UV CD spectra (**b**) of *Ps*BGAL treated with 0, 1.9, 3.7, and 6 M GdnHCl at pH 5, respectively. **c** Effect of GdnHCl on ANS binding of *Ps*BGAL at pH 5.0. *Ps*BGAL was treated with GdnHCl at concentration of 0, 1.9, 3.7, and 6 M at pH 5.0

Enzyme has percentage of α and β content of 33.6±2.8 and 26.6±1.0, respectively, as found from secondary structure studies using far-UV CD spectra (Table 1). λ_{max} corresponds to 346.59 and 488.67 nm as found by intrinsic Trp fluorescence and ANS binding studies (see "Changes in Intrinsic Fluorescence" and "Exposure of Hydrophobic Clusters and Patches" sections).

First intermediate (I_1) It resembled to monomeric state of *N* state with molecular mass of 61.0 kD (data not shown). Enzyme activity of I_1 state was lesser than that of *N* state by 29%. Amount of secondary structures present in the first intermediate was entirely different as that of *Ps*BGAL at pH 8.0 (existing as monomer, molecular mass of 57.0 kD; Tables 1 and 3). These studies indicated that monomeric first intermediate (I_1) has higher β content than monomeric *Ps*BGAL at pH 8.0. I_1 state has retained its tertiary structure as observed by the presence of positive peak centered at 278 nm and a negative peak between 298 and 300 nm as observed by near-UV CD spectra (Fig. 6b). There was a red shift of ~7 nm with decrease in fluorescence intensity by 36% corresponding to intrinsic Trp fluorescence (data not shown). ANS fluorescence binding studies have revealed that I_1 state has least exposed hydrophobic clusters as there was drastic decrease in ANS fluorescence intensity by ~28% (Fig. 6c). Obtained conformational free energy change during the process $N \leftrightarrow I_1$ was quite low corresponding to involvement of weak interactions during the process of multimerization (Table 2). It can be concluded from these studies that subsequent unfolding of multimeric *Ps*BGAL in the presence of GdnHCl has led to its monomerization. Further, monomerization was accompanied with exposure of Trp residues with least exposed hydrophobic clusters. Multimerization of enzyme is due to interfacial interactions of individual units containing residues like Trp as key determining factor rather than hydrophobic interactions in support with "Changes in Intrinsic Fluorescence" and "Exposure of Hydrophobic Clusters and Patches" sections. Moreover, higher β content in I_1 than in monomeric *Ps*BGAL at alkaline pH might have imparted additional intermolecular interactions for enzyme multimerization. Extensive studies on protein–protein interactions have also revealed that hydrophobic interactions have least significance [40]. Further, Trp residue has the greatest conservation propensity at hot spots region involve in the interaction, due to its large size and aromatic nature [41].

Second intermediate (I_2) This state has completely lost its tertiary structure (near-UV CD, Fig. 6b) in accordance with complete loss in enzyme activity, while secondary structures present in the enzyme were retained (Fig. 6a). Comparative analyses based on retention of secondary structures have revealed that there was a loss of 67% in α-helical content while no loss in β-content (Table 3). Qualitative analyses of far-UV CD spectra of state I_2 (Fig. 6a) showed that enzyme has all β-content in contrast to native state *N* containing α/β structures. It can be concluded that enzyme has an active site situated at α/β structures,

Table 3 Percent of secondary structures of native and intermediate *Ps*BGAL in transition states.

% Secondary structures	Native (*N*)	Intermediate (I_1)	Intermediate (I_2)
α-Helix	33.6±2.8	27.2±2.1	11.2±0.7
β-Sheet	26.6±1.0	36.0±2.4	39.9±2.3
Turns	11.0±1.3	9.8±1.4	9.8±0.5
Random coil	28.8±2.1	26.9±1.9	39.0±2.9

The content of secondary structures was calculated from CD data by SOMCD program.

while there was presence of other domain, which is rich in β-content and devoid of enzyme activity. Conformational free energy change from state $I_2 \leftrightarrow U$ was 13.95 kcal moL^{-1} M^{-1}, while from state $I_1 \leftrightarrow I_2$, it was 11.03 kcal moL^{-1} M^{-1} (Table 2). Thus, state I_2 was more stable and resistant to unfolding by GdnHCl with respect to state I_1. It could be anticipated that this β-rich domain might be playing important role during enzyme multimerization, thus responsible for its stability. Intrinsic Trp fluorescence studies have revealed a red shift of ~8 nm with respect to *N* state (data not shown). Further, studies by ANS binding have revealed that state resembled to molten globule corresponding to the blue shift of ~40 nm with respect to I_1 state within ANS fluorescence intensity by ~60% (Fig. 6c).

Unfolded state (U) State corresponds to complete loss of tertiary structures (near-UV CD, Fig. 6b), enzyme activity, and α-helical content (far-UV CD, Fig. 6a). λ_{max} was found to be 355.47 nm corresponding to Trp emission, resembling completely unfolded protein. Further, a red shift of ~30 nm was observed by ANS binding studies with respect to state I_2 (Fig. 6c). Thus, *Ps*BGAL denaturation pathway can be indicated by the following scheme:

$$\textbf{Tetramer}(N) \rightarrow \textbf{Monomer}(I_1) \rightarrow \textbf{Molten globule}(I_2) \rightarrow \textbf{Completely unfolded}(U)$$

Unfolding Studies at Alkaline pH

Unfolding studies of *Ps*BGAL using GdnHCl at pH 8.0 were monitored using changes in helical content, intrinsic Trp fluorescence intensity, and enzyme activity. The percentage of α-helicity approaches to negligible, as *Ps*BGAL was completely unfolded with complete loss of enzyme activity and λ_{max} corresponding to intrinsic Trp emission approaches to 355 nm. A plot was generated based on Eqs. 3 and 4 ("Materials and Methods" section), with fraction unfolded (f_u) versus varying GdnHCl concentration from 0 to 6 M based on loss in percentage of α-helicity, loss in enzyme activity, and decrease in intrinsic Trp fluorescence intensity corresponding to emission wavelength at 355 nm. Data obtained from far-UV CD, intrinsic Trp fluorescence, and enzyme activities were fitted based on two-state model (Eq. 19). Denaturation curve obtained by the three studies were found to be cooperative and coincidental with transition mid-points corresponding to 1.5, 1.78, and 2.25 M by enzyme activity, intrinsic Trp fluorescence studies, and secondary structure studies (far-UV CD), respectively (Fig. 5b). Thermodynamic parameters obtained from linear extrapolation models described in "Materials and Methods" section (Eqs. 14–17) are given in Table 2. These studies revealed that secondary structure of *Ps*BGAL was much resistant to denaturation by GdnHCl with respect to its tertiary structure. Furthermore, comparative analyses of thermodynamic parameters at pH 5.0 and 8.0 have found that *Ps*BGAL has higher stability at acidic pH than at higher pH.

Conclusion

*Ps*BGAL is the resident of acidic environment (inside vacuoles) under *in vivo* conditions. Enzyme has unique tendency of multimerization at acidic conditions despite the absence of lectin domain. The phenomenon of multimerization was the function of protein concentration and pH of the solution. Multimerization helps the enzyme in its stabilization under acidic and further enhances its activity. Here, we observed through biophysical characterization of multimeric *Ps*BGAL that enhanced protein concentrations (>100 μg mL^{-1}) lead to its

multimerization. Thus, protein–protein interactions play crucial role in stabilization, retention of tertiary structures, and enzyme activity. The protein concentration of *Ps*BGAL was found to play a crucial role in multimerization of enzyme. Gibbs free energy change corresponding to monomerization of *Ps*BGAL in the presence of GdnHCl was 2.57 kcal moL^{-1} M^{-1} (quite low).

Fungal BGAL has been commercially exploited for oral enzyme therapy in treatment of lactose intolerance due to its higher stability towards acidic conditions as compared to bacterial BGAL to resist the gastric environment of the stomach. *Ps*BGAL isolated from pea (*P. sativum*) has been found to have higher affinity towards lactose than fungal BGAL [17]. The present work concludes that the enzyme has higher stability under acidic conditions, with protein concentrations ≥100 μg mL^{-1}. Therefore, *Ps*BGAL presents a potential substitute for fungal BGAL in commercial applications due to its plant origin (easy adaptability towards human), stability towards acidic conditions, high affinity towards lactose, and cheap and easier accessibility.

Acknowledgement A.D. would like to thank the Council of Scientific and Industrial Research (CSIR), New Delhi for financial assistance in the form of research fellowship.

References

1. Dwevedi, A., & Kayastha, A. M. (2009). *Journal of Agricultural and Food Chemistry, 57*, 7086–7096.
2. Dwevedi, A., & Kayastha, A. M. (2009). *Journal of Agricultural and Food Chemistry, 57*, 682–688.
3. Uhrig, J. F., Soellick, T.-R., Minke, C. J., Philipp, C., Kellmann, J.-W., & Schreier, P. H. (1999). *Proceedings of the National Academy of Sciences of the United States of America, 96*, 55–60.
4. Dubey, V. K., Pande, M., Singh, B. K., & Jagannadham, M. V. (2007). *African Journal of Biotechnology, 6*, 1077–1086.
5. Heyworth, C. M., Neumann, E. F., & Wynn, C. H. (1981). *Biochemical Journal, 193*, 773–779.
6. Hoogeveen, A. T., Verheijen, F. W., & Galjaard, H. (1983). *The Journal of Biological Chemistry, 258*, 12143–12146.
7. Potier, M., Michaud, L., Tranchemontagne, J., & Thauvette, L. (1990). *The Biochemical Journal, 267*, 197–202.
8. Yamamoto, Y., Fujie, M., & Nishimura, K. (1982). *Journal of Biochemistry, 92*, 13–21.
9. Pridham, J. B., & Dey, P. M. (1984). In A. Meister (Ed.), *Advances in enzymology & related areas of molecular biology* (Vol. 56, pp. 83–96). New York: Wiley.
10. Sue, M., Yamazaki, K., Yajima, S., Nomura, T., Matsukawa, T., Iwamura, H., et al. (2006). *Plant Physiology, 141*, 1237–1247.
11. Strasser, R., Bondili, J. S., Schoberer, J., Svoboda, B., Liebminger, E., Glössl, J., et al. (2007). *Plant Physiology, 145*, 5–16.
12. Frandsen, T. P., Lok, F., Mirgorodskaya, E., Roepstorff, P., & Svensson, B. (2000). *Plant Physiology, 123*, 275–286.
13. Dey, P. M., Campillo, E. M. D., & Lezica, R. P. (1983). *The Journal of Biological Chemistry, 258*, 923–929.
14. Dey, P. M., Pridham, J. B., & Sumar, N. K. (1982). *Phytochemistry, 21*, 180–186.
15. Dey, P. M. (1984). *European Journal of Biochemistry, 140*, 385–390.
16. Goldstein, U., Hughes, R. C., Monsigny, M., Osawa, T., & Sharon, N. (1980). *Nature, 285*, 66.
17. Nallamsetty, S., Dubey, V. K., Pande, M., Ambasht, P. K., & Jagannadham, M. V. (2007). *Biochimie, 89*, 1416–1424.
18. Fernandez, A., & Scheraga, H. A. (2003). *Proceedings of the National Academy of Sciences of the United States of America, 100*, 113–118.
19. Clackson, T., & Wells, J. A. (1995). *Science, 267*, 383–386.
20. Bogan, A. A., & Thorn, K. S. (1998). *Journal of Molecular Biology, 280*, 1–9.
21. Ma, B., Elkayam, T., Wolfson, H., & Nussinov, R. (2003). *Proceedings of the National Academy of Sciences of the United States of America, 100*, 5772–5777.
22. Levy, Y., Wolynes, P. G., & Onuchic, J. N. (2004). *Proceedings of the National Academy of Sciences of the United States of America, 101*, 511–516.

23. Schmid, F. X. (1998). In T. Creighton (Ed.), *Protein structure, a practical approach* (pp. 261–296). New York: IRL Press.
24. Bradford, M. M. (1976). *Analytical Biochemistry, 72*, 248–254.
25. Balasubramanian, D., & Kumar, C. (1976). *Applied Spectroscopy Reviews, 11*, 223–286.
26. Semisotnov, G. V., Rodionova, N. A., Razgulyaev, O. I., Uversky, V. N., Gripas, F., & Gilmanshin, R. I. (1991). *Biopolymers, 31*, 119–128.
27. Khurana, R., & Udgaonkar, J. B. (1994). *Biochemistry, 33*, 106–115.
28. Park, Y. C., & Bedouelle, H. (1998). *The Journal of Biological Chemistry, 273*, 18052–18059.
29. Manavalan, P., & Johnson, W. C. (1983). *Nature, 305*, 831–832.
30. Golczak, M., Kicinska, A., Pikula, J. B., Buchet, R., Szewczyk, A., & Pikula, S. (2001). *The FASEB Journal, 15*, 1083–1085.
31. Carneiro, F. A., Ferradosa, A. S., & Da Poian, A. T. (2001). *The Journal of Biological Chemistry, 276*, 62–67.
32. Ruano, M. L. F., Pérez-Gil, J., & Casals, C. (1998). *The Journal of Biological Chemistry, 273*, 15183–15191.
33. Gasset, M., Baldwin, M. A., Fletterick, R. J., & Prusiner, S. B. (1993). *Proceedings of the National Academy of Sciences of the United States of America, 90*, 1–5.
34. Zhou, N. E., Mant, C. T., & Hodges, R. S. (1990). *Peptide Research, 3*, 8–20.
35. Tsai, C. J., Lin, S. L., Wolfson, H. J., & Nussinov, R. (1997). *Protein Science, 6*, 53–64.
36. Halfman, C. J., & Nishida, T. (1971). *Biochimica et Biophysica Acta, 243*, 294–303.
37. Dahms, T. E. S., & Szabo, A. G. (1995). *Biophysical Journal, 69*, 569–576.
38. Matulis, D., & Lovrien, R. (1998). *Biophysical Journal, 74*, 422–429.
39. Pace, C. N. (1975). *Critical Reviews in Biochemistry, 3*, 1–43.
40. Brinda, K. V., & Vishveshwara, S. (2005). *BMC Bioinformatics, 6*, 296–311.
41. Jones, S., & Thornton, J. M. (1996). *Proceedings of the National Academy of Sciences of the United States of America, 93*, 13–20.